Growing self-assisted GaAs nanowires up to 80 μm long by Molecular Beam Epitaxy

Jeanne Becdelievre, Xin Guan, Iuliia Dudko, Philippe Regreny, Nicolas Chauvin, Gilles Patriarche, Michel Gendry, Alexandre Danescu, Jose Penuelas

Growing self-assisted GaAs nanowires up to 80 µm long by Molecular Beam Epitaxy

Jeanne Becdelievre[1], Xin Guan[1], I. Dudko[1, 2, 3], Philippe Regreny[1], Nicolas Chauvin[1], Gilles Patriarche[4], Michel Gendry[1], Alexandre Danescu[1], José Penuelas[1]

[1] Univ Lyon, Ecole Centrale de Lyon, CNRS, INSA Lyon, Université Claude Bernard Lyon, CPE Lyon, INL, UMR5270, 69130 Ecully, France
[2] School of Engineering, RMIT University, Melbourne 3001, Victoria, Australia
[3] Functional Materials and Microsystems, Research Group and Micro Nano Research Facility, RMIT University, Melbourne 3001, Victoria, Australia
[4] Centre de Nanosciences et de Nanotechnologies - C2N, CNRS, Université Paris-Sud, Université Paris-Saclay, 91120 Palaiseau, France

* To whom correspondence should be addressed. E-mail: jose.penuelas@ec-lyon.fr

KEYWORDS: ultra-long nanowires, Molecular beam epitaxy, VLS growth

ABSTRACT: Ultralong GaAs nanowires were grown by molecular beam epitaxy using the vapor-liquid-solid method. In this ultralong regime we show the existence of two features concerning the growth kinetic and the structural properties. Firstly, we observed a non-classical growth mode, where the axial growth rate is attenuated. Secondly, we observed structural defects at the surface of Wurtzite segments located at the bottom part of the nanowires. We explain these two phenomena as arising from a particular pathway of the group V species, specific to ultralong nanowires. Finally, the optical properties of such ultralong nanowires are studied by photoluminescence experiments.

1. Introduction:

Ultra-long semiconducting nanowires (NWs) can be of interest for applications which require large length or large active areas, such as sensors [**Cui 2001**, **Thelander 2006**] or water splitting [**Kamimura 2017**]. Various methods have been used to fabricate ultra-longs NWs, as for example electrospinning for ZnO [**Wu 2006**], CVD for ZnO [**Li 2008**], Si [**Kayes 2007**] or III-V [**Kim 2008**], HVPE for GaAs [**Ramdani 2010**] or GaN [**Avit 2014**]. Due to its low growth rate, Molecular Beam Epitaxy (MBE), is rarely used to grow ultra-long NWs, whereas it allows integration on Si substrates of various semiconductors with high purity and a good verticality.

GaAs, due to its direct bandgap and its high carrier mobility, is a promising material for solar energy harvesting with photovoltaics [**Vettori 2019**] or photoelectrodes [**Hu 2013, Cui 2021**], the NW geometry leading to an efficient light trapping. More recently it was demonstrated GaAs NWs can be used as templates for the growth of hexagonal Germanium [**Fadaly 2020**, **Dudko 2021**]. However, the maximal reported length of GaAs NWs grown by MBE, at the best of our knowledge, is about 25 µm [**Braakman 2014**] and typical growth time rarely exceeds 2 hours [**Zhou 2017**]. Achieving ultra-long NWs only requires to maintain the Vapor-Liquid-Solid (VLS) mechanism during the growth, which means to prevent the crystallization of the catalyst droplets. However, this can be challenging in the case of the self-assisted NWs since when reaching the ultra-long regime, the growth mechanism becomes more complex due to phenomena, such as molecular flux shadowing, becoming predominant and/or due to significant variations of the temperature appearing at the NW tip.

The aim of this work is to study the properties of ultra-long nanowires grown by MBE. In particular, we focus on the NW growth kinetic and their structural and optical properties. By prolonging the MBE growth time we achieve a maximum length of 80 µm for self-assisted GaAs NWs grown on Si.

2. Nanowire growth

Self-assisted GaAs NWs have been grown on N-doped Si(111) substrates by solid source MBE. Before being introduced in ultrahigh vacuum, the epi-ready Si substrates were cleaned for 5 min with ultrasonic waves in acetone then in ethanol in order to remove surface contaminations. Substrates were then outgassed in ultrahigh vacuum for 20 min at 200°C. GaAs NWs were grown in a Riber MBE reactor dedicated to III-V semiconductors equipped with a Reflection High Energy Electron Diffraction (RHEED) facility. The MBE reactor is equipped with a Ga cell with a flux incidence angle equal to 27.9°, and an As_4 valved cracker cell with a flux incidence angle equal to 41° [**Vettori 2019b**]. The substrate temperature was controlled by a calibrated thermocouple and checked by a pyrometer. During growth the sample holder was continuously rotated to enhance the growth homogeneity. Self-assisted GaAs NWs were grown by MBE using the VLS method with Ga droplets [**Foncuberta 2008, Jabeen 2008, Ramdani 2013, Priante 2013, Matteini 2015, Dubrovskii 2015, Guan 2016a, Guan 2016b**]. First, the Si substrate temperature was increased to 500°C and 1 monolayer of Ga was deposited at a deposition rate of 1.4 Å/s on the substrate which was still covered by its 2 nm-thick native oxide layer. Then, the substrate temperature was increased up to the growth temperature at 610°C. During this step, Ga droplets react with the oxide layer to form volatile oxides with the formation of holes [**Matteini 2015, Fouquat 2019**]. It allows the epitaxial growth of the GaAs NWs on the Si substrate [**Bailly 2022**]. The Ga flux used for the NW growth was 2.1 Å/s in unit of equivalent 2D GaAs growth rate [**Rudolph 2011**] and the As_4 beam equivalent pressure was set at $7.6x10^{-6}$ mbar which corresponds to a As/Ga flux ratio of 4.8. Ga shutter and As valve were opened at the same time to initiate the NW growth and closed simultaneously in order to avoid the crystallization of the droplet and to confirm the VLS process.

Growths were carried out for various durations, from 5 min to 12 hours. A representative SEM image of the NWs grown for 12 hours is shown in figure 1(a). The GaAs NWs are almost all

vertical (see the SEM images of the Supporting Information section). We can also notice in figure 1(a) that two groups of NWs are present. NWs from the first group still have a Ga droplet on the top, as illustrated on figure 1(b). The diameter of the Ga droplet is around 1 µm and the length of the NWs is about 80 µm. These NWs present a strong inverted tapering with a diameter increasing from 80 nm at the base to 700 nm just underneath the droplet. NWs from the second group, observable on figure 1(c), exhibit a facetted crystal on the top. For these NWs, the VLS process has not been kept during the whole growth. The droplet has crystallized during the process, stopping the axial growth. The origin of this crystallization phenomena could be the consequence of a strong V/III ratio supply in the droplet. The origin of the droplet crystallization is not clear and is not studied in this study. In the rest of this article, we are only interested by the first group of NWs which are representative of the VLS process.

3. Growth kinetic of ultralong NWs

The evolutions of the NW length and diameter as a function of the growth time can be seen on the figure 2(a). For growth times shorter than 2 hours, the relation between the NW length and the growth time is linear, as expected for the VLS process [**Colombo 2008**]. However, the slope of the curve changes at 2 hours. The decrease of the growth rate of long NWs is not expected by the Glas *et al.* model [**Glas 2013**]. To examine furthermore this phenomenon, we plot the axial growth rate as a function of the radius of the NWs beneath the droplet. Glas' model predicts an almost stationary axial growth rate for radii between 50 and 100 nm and even if larger radii haven't been studied, a similar behavior is expected. As we can see on figure 2(b), we have a different result. For radii larger than 100 nm, the axial growth rate drops. The classical scenario of a self-regulated evolution of the NW growth is based on the following arguments: in the Ga-rich regime, since the droplet radius increases and the V/III ratio is always larger than 1, the amount of As entering the droplet by direct impingement will stabilize the droplet size so as to obtain a stationary growth regime (here by stationary growth regime we

understand constant axial growth rate at a fixed NW diameter). At the opposite, in a Ga-poor regime, the droplet radius decreases so that both Ga and As quantities entering the droplet by direct impingement decrease. But the droplet radius variation does not affect the amount of Ga feeding the droplet via the diffusion along the NW facets so that this contribution will also stabilize the droplet radius. However, small deviations from the stationary growth regime cannot be observed at short growth times. Experimental data in figure 2 provide a straightforward way to compute the amount of Ga and As atoms which participate to the solidification process in the $[t_i,\ t_{i+1}]$ time interval. In the following, to obtain good accuracy, we use linear interpolation of the experimental data with a fixed time-step Δt = 432 s. From the experimental data we compute the solid volume grown in the $[k\Delta t, (k+1)\Delta t]$ time interval by using the interpolated values for the NW radius and NW length. Obviously, the amount of solid volume grown in the $[k\Delta t, (k+1)\Delta t]$ time interval is $\Delta V_k = \frac{\pi}{3}(L_{k+1} - L_k)(r_k^2 + r_k r_{k+1} + r_{k+1}^2)$ and this can be further converted so as to obtain the (equal) amount of Ga and As atoms that participate to the solidification process in the $[k\Delta t, (k+1)\Delta t]$ time interval. But the tappering observed during the growth (see figure S1(d)) shows that the droplet contact angle is fixed at its maximum value in which case, from the NW radius, we can compute the droplet radius at $t_k = k\Delta t$ further denoted R_k. Using the droplet radius and the NW radius we compute the (time-dependent) area of the free-surface of the droplet S_k^{drop} intercepted by the flux and we can check the correlation between the free-surface of the droplet and the equal amount of Ga and As atoms used for solidification in the $[k\Delta t, (k+1)\Delta t]$ time interval. Figure 3 shows an excellent correlation between these two quantities obtained for a constant value of the As (and Ga) flux of 1.7×10^7 atoms/ (nm².s) in the [0, 115 min] time range. We can conclude the quantity of As which participate to the growth is directly proportional to the droplet surface. By consequence, incorporated As is only originated from the droplet and not from the diffusion along the facets.

However, the remaining experimental data do not fit this short-time behavior and the deviation needs an interpretation. Several explanations can be put forward: the temperature at the top of the NW (i), the droplet morphology (ii) and the incorporation of arsenic in the droplet (iii).

(i) For ultra-longs NWs the temperature isn't homogenous along the NW and a temperature drop of about 50 K can be expected (see details in Supporting Information section). Yet, a temperature drop should induce an increase of the growth rate [**Glas 2013**], so it cannot explain the observed specific growth kinetic of ultra-long NWs. However, it should be noted that if we consider a mechanism of As diffusion on the GaAs facets as suggested by Scarpellini *et al.* [**Scarpellini 2017**], then the temperature drop would induce a decrease of the As diffusion and consequently a decrease of the axial growth rate. However this additional source of elementary As is expected to occur at temperatures of about 400°C, which is significantly different from our calculation (see figure 3). Consequently, in the following of this article we will consider that elementary As is desorbed from the GaAs surface during the VLS growth.

(ii) The ultra-longs nanowires presented here have a very large droplet, with a diameter larger than 1 µm. A calculation has been carried out to check if arsenic diffusion length is sufficient to reach the liquid-solid interface where the growth occurs. To do this, we have calculated the length $L=\sqrt{D\tau_c}$ covered by an arsenic atom in the droplet during $\tau_c = 0.1$ s, the time needed to create one monolayer of GaAs. We have used the Stokes-Einstein equation to determine an approximated value of the diffusion coefficient D of arsenic in liquid gallium:

$$D = \frac{k_B T}{6\pi\, r_{As}\ \mu_{Ga}} \sim 6.0 \times 10^{-5} cm^2\, s^{-1} \qquad \text{(eq1)}$$

The computed value is coherent with already obtained results in [**Gorokhov 1984**]. In this equation, k_B is the Boltzmann coefficient, T the temperature, r_{As} the radius of the arsenic atom and μ_{Ga} the gallium viscosity [**Spells 1936**]. At last, we found a length L $\sim 25\ \mu m$ considerably larger than the droplet diameter. This result is in good agreement with previous results on gold-assisted growth of silicon NWs where it has been shown that whatever the diameter of the droplet, the growth rate is stationary [**Kodambaka 2006**].

(iii) Among the arguments advanced in the literature the retro-diffusion of As was mentioned in [**Ramdani 2013**]. In this model, arsenic atoms reemitted from other NWs and substrate incorporate the droplet to participate to the axial growth. Due to its large length, a strong screening effect occurs and arsenic atoms could not reach the droplet and only participate to the radial growth. It would explain the growth rate drop when the growth time increases. From a qualitative point of view the correlation between the As amount needed for the solidification and the time evolution of the droplet free surface area may be explained as follows: when the length of the NW scales as t^{α} and the radius of the NW scales as t^{β} the amount of As (or Ga) atoms in a small time-interval scales like $t^{\alpha+2\beta-1}$. Meanwhile at constant wetting angle the radius of the droplet scales like t^{β} so that the free-surface area of the droplet scales like $t^{2\beta}$. An excellent correlation is then obtained only when $\alpha = 1$, which is the case in the short-time behaviour. From a quantitative point of view we notice a significant variation of the amount of As (and Ga) atoms needed for the NW growth process: from 50.1×10^6 atoms/s at the beginning of the growth to 76.7×10^8 atoms/s after 10 hours. Compared to this, the deficit of As entering the droplet varies from 37.2×10^3 atoms/s at the beginning of the growth to 10.4×10^5 atoms/s after 10 hours. Thus, since the As deficit (or Ga Excess) is three order

of magnitude lower than the amount of atoms entering the solidification process, only long-time growth experiments can obtain evidence of it.

4. Structure and optical properties

TEM characterizations have been lead on ultra-long GaAs NWs. The structure of the NWs is mostly Zinc Blende (ZB). The base of the NWs is purely ZB, twins appear after several microns and their density is increasing along the NWs, as it can be seen on figure 4(a). Near the top, Wurtzite (WZ) inclusions appear, as shown on figure 4(b) and a large WZ segment is present underneath the droplet [**Dursap 2020]**. The presence of two crystal phase in self-assisted GaAs NWs is well known [**Panciera 2020**] and can be in a certain extent controlled [**Dursap 2021**] in order to obtain desired properties [**Li 2021**]. These ultra-long NWs also present crystallographic particularities. In the middle of the NWs, we found notches on the ridges of the NWs, as we can observe on figure 4(c). A WZ segment can be noticed at each notch, see figure 4(d). The WZ segment seems to be a point of departure of the notches formation. We think these defects are the consequence of the GaAs decomposition due to the high growth temperature and the lack of arsenic already highlighted via the discussion on the growth kinetic. At the bottom of the NWs, we found holes with an increasing density near the base, see figure 4(e). In the area where the hole density is low, these defects are aligned perpendicularly to the growth axis. Recently, thanks to *in situ* TEM experiments it was found that during heating of GaAs NWs, the WZ phase evaporates before the ZB one [**Gang 2021**]. It can thus be noted that the holes are formed at the NW foots which are pure ZB phase. In our case, the lack of As could explain this phenomenon, since the congruent evaporation temperature of GaAs is directly controlled by the As molecular flux [**Zhou 2012**]. In order to confirm this hypothesis we performed VLS growth of ultralong NWs under As-rich condition and low density (see figure S6). The NWs grown under As-rich condition do not show any structural defects from SEM

observation, and no tapering is observed, which means the ultralong NWs morphology and structure can be partially controlled by tuning the V/III ratio during the growth.

The photoluminescence (PL) measurements are performed in a closed cycle cryostat, using a 532 nm continuous wave laser as the excitation source and a liquid nitrogen cooled silicon CCD detector coupled to a monochromator for the detection. To investigate the dynamics, time-resolved measurements were performed at 14 K using a 200-fs pulsed laser emitting at 515 nm with a 54 MHz repetition rate. The PL of the NWs is analyzed by a spectrometer and a synchronized streak camera with a temporal resolution of 20 ps. PL measurements are performed on the as-grown sample. Therefore, the laser is completely absorbed in the upper part of these ultra-long NWs. PL performed at 12 K reveals a single peak whose energy blueshifts from 1.442 eV to 1.447 eV along with the excitation power increase (see figure 5 (a)). This peak is clearly below the exciton emission in ZB GaAs (1.516 eV) and WZ GaAs (1.524 eV) as reported in [**Dursap 2021**]. Moreover, the PL dynamics reveal a decay time longer than 10 ns (see figure 5 (b)). If the inhibition of the radiative lifetime is possible in high refractive index materials [**Claudon 2013**], the diameter of the investigated NWs discards this hypothesis. The long decay time, the emission below the band gap and the PL blueshift are signatures of carrier separations induced by the WZ-ZB phase mixing, in agreement with the TEM results, which creates a type II band alignment in GaAs NWs [**Heiss 2011**, **Vainorius 2014**, **Vainorius 2015**]. The observation of a PL emission centered between 1.44 eV and 1.45 eV is associated to relatively thick WZ insertions: in Ref [**Vainorius 2015**], these energies were obtained for 2 to 3 nm long WZ GaAs QDs in ZB GaAs NWs. These lengths agree with the length of the WZ insertions measured by TEM where the notches are observed. The PL emission was also investigated as a function of the temperature (see figure S4), revealing a typical character of unpassivated GaAs NWs. Then, micro-photoluminescence experiments were performed to investigate the optical properties at the single NW level. GaAs NWs have

been transferred on a TEM grid and inserted into a low-vibration closed cycle cryostat. For theses measurement, a cw 671 nm laser with a 5 µm spot size and a power of 500 µW was used for the excitation and a liquid nitrogen cooled silicon CCD detector coupled to a monochromator for the detection. Fig 5 (c) shows the µ-PL spectrum of a single GaAs NW excited in the center where several peaks are observed. The low energy peak at 1.431 eV is associated to the thick WZ GaAs insertions as observed in the PL experiments. Other peaks are observed at higher energy up to 1.491 eV. These peaks are associated to thinner WZ insertions. For instance, Martin Heiss *et al* report a µ-PL emission in the 1.49-1.5 eV range for 2-3 ML-thick WZ GaAs insertions [**Heiss 2011**], whereas Bolinnsson et al observed a peak at 1.48 eV related to rotational twins [**Bolinsson 2014**]. No emission associated to the ZB GaAs is observed which can be explained by a high density of WZ insertions and twins: in Ref [**Bolinsson 2014**], pure ZB GaAs segments longer than 35 nm were required to observe the free exciton emission from ZB GaAs at cryogenic temperature.

5. Conclusion and perspectives:

In conclusion, we have managed to growth ultra-long GaAs nanowires by MBE. We have noticed a decrease of the growth rate after 2 hours of growth and attributed this phenomenon to a lack of arsenic in the droplet due to a screening effect and to radial growth. This lack of arsenic seems also at the origin of notches and holes in the nanowires. To confirm this hypothesis, *in situ* heating experiments as in ref [**Fouquat 2021**] could be performed. It should be noted that for application with ultra-long GaAs nanowires a particular attention has to be given to the degradation on the bottom of the nanowires due to the possible lack of Arsenic.

Acknowledgements:

Chinese Scholarship Council (CSC) is acknowledged for its financial support. The authors thank the NanoLyon platform for access to equipment, J. B. Goure for technical assistance.

References:

[**Avit 2014**] Avit, G., Lekhal, K., André, Y., Bougerol, C., Réveret, F., Leymarie, J., ... & Trassoudaine, A. Nano letters, 14(2), 559-562. (2014)

[**Bailly 2022**] L. Bailly-Salins, M. Vettori, T. Dursap, P. Regreny, G. Patriarche, M. Gendry, J. Penuelas, A. Danescu, Crystal Growth & Design (2022) doi.org/10.1021/acs.cgd.2c00685

[**Bolinsson 2014**] J. Bolinsson, Martin Ek, J. Trägårdh1, K. Mergenthaler, D. Jacobsson, M.-E. Pistol, L. Samuelson, A. Gustafsson, Nano Research 7, 473–490 (2014)

[**Braakman 2014**] Braakman, F. R., Cadeddu, D., Tütüncüoglu, G., Matteini, F., Rüffer, D., Fontcuberta i Morral, A., & Poggio, M. Applied physics letters, 105(17), 173111. (2014)

[**Claudon 2013**] J. Claudon, N. Gregersen, P. Lalanne, J.-M. Gérard, Chemphyschem 14, 2393-2402 (2013)

[**Colombo 2008**] Colombo, C., Spirkoska, D., Frimmer, M., Abstreiter, G., & i Morral, A. F. Physical Review B, 77(15), 155326. (2008)

[**Cui 2001**] Y. Cui, C. M. Lieber, Science 291, 851 (2001)

[**Cui 2021**] Fan Cui, Yunyan Zhang, H. Aruni Fonseka, Premrudee Promdet, Ali Imran Channa, Mingqing Wang, Xueming Xia, Sanjayan Sathasivam, Hezhuang Liu, Ivan P. Parkin, Hui Yang, Ting Li, Kwang-Leong Choy, Jiang Wu, Christopher Blackman, Ana M. Sanchez, and Huiyun Liu, ACS Appl. Mater. Interfaces 13, 30950 (2021)

[**Dubrovskii 2015**] V. G. Dubrovskii, T. Xu, A. Diaz-Alvarez S. R. Plissard, P. Caroff, B. Grandidier, Nano Letters 15, 5580 (2015)

[**Dudko 2021**] I. Dudko, T. Dursap, A. D. Lamirand, C. Botella, P. Regreny, A. Danescu, S. Brottet, M. Bugnet, S. Walia, N. Chauvin, J. Penuelas, Crystal Growth & Design 22, 32 (2022)

[**Dursap 2020**] T. Dursap, M. Vettori, A. Danescu, C. Botella, P. Regreny, G. Patriarche, M. Gendry, J. Penuelas, Nanoscale Advances 2, 2127 (2020)

[**Dursap 2021**] T. Dursap, M. Vettori, C. Botella, P. Regreny, N. Blanchard, N. Chauvin, M. Gendry, M. Bugnet, A. Danescu, J. Penuelas, Nanotechnology 32, 155602 (2021)

[**Fadaly 2020**] E. M. T. Fadaly et al. Nature 580, 205 (2020)

[**Fontcuberta 2008**] A. Fontcuberta i Morral, C. Colombo, G. Abstreiter, Appl. Phys. Lett. 92, 063112 (2008)

[**Fouquat 2019**] L. Fouquat, M. Vettori, C. Botella, A. Benamrouche, J. Penuelas, G. Grenet, Journal of Crystal Growth 514, 83 (2019)

[**Fouquat 2021**] L. Fouquat, X. Guan, C. Botella, G. Grenet, P. Regreny, M. Gendry, H. Yi, J. Avila, M. Bugnet, J. Penuelas, Journal of Physical Chemistry C 125, 28136 (2021)

[**Glas 2006**] Glas, F., & Harmand, J. C. Physical Review B, 73(15), 155320 (2006)

[**Glas 2013**] Glas, F., Ramdani, M. R., Patriarche, G., & Harmand, J. C. Physical Review B, 88(19), 195304 (2013)

[**Gorokhov 1984**] Gorokhov, V. A., Dedegkaev, T. T., Ilyin, Y. L., Moshnikov, V. A., Petrov, A. S., Sosov, Y. M., & Yaskov, D. A. Crystal research and technology, 19(11), 1465 (1984)

[**Guan 2016a**] X. Guan, J. Becdelievre, B. Meunier, A. Benali, G. Saint-Girons, R. Bachelet, P. Regreny, C. Botella, G. Grenet, N. P. Blanchard, X. Jaurand, M. G. Silly, F. Sirotti, N. Chauvin, M. Gendry, J. Penuelas, Nano Letters 16, 2393 (2016)

[**Guan 2016b**] X. Guan, J. Becdelievre, A. Benali, C. Botella, G. Grenet, P. Regreny, N. Chauvin, N. P. Blanchard, X. Jaurand, G. Saint-Girons, R. Bachelet, M. Gendry, J. Penuelas, Nanoscale 8, 15637 (2016)

[**Gang 2021**] Geun Won Gang, Jong Hoon Lee, Su Yeon Kim, Taehyeon Jeong, Kyung Bin Kim, Nguyen Thi Hong Men, Yu Ra Kim, Sang Jung Ahn, Chung Soo Kim and Young Heon Kim, Nanotechnology 32, 145709 (2021)

[**Heiss 2011**] M. Heiss, S. Conesa-Boj, J. Ren, H.-H. Tseng, A. Gali, A. Rudolph, E. Uccelli, F. Peiro, J. R. Morante, D. Schuh, E. Reiger, E. Kaxiras, J. Arbiol, A. Fontcuberta i Morral, Physical Review B 83, 045303 (2011).

[**Hu 2013**] Shu Hu, Chun-Yung Chi, Katherine T. Fountaine, Maoqing Yao, Harry A. Atwater, P. Daniel Dapkus, Nathan S. Lewis, Chongwu Zhou, Energy Environ. Sci. 6, 1879 (2013)

[**Jabeen 2008**] F. Jabeen, V. Grillo, S. Rubini, F. Martelli, Nanotechnology 19 275711 (2008)

[**Kamimura 2017**] Kamimura, J., Bogdanoff, P., Ramsteiner, M., Corfdir, P., Feix, F., Geelhaar, L., & Riechert, H. Nano Letters, *17*(3), 1529 (2017)

[**Kayes 2007**] Kayes, B. M., Filler, M. A., Putnam, M. C., Kelzenberg, M. D., Lewis, N. S., & Atwater, H. A. Applied Physics Letters, 91(10), 103110 (2007)

[**Kim 2006**] Kim, Y., Joyce, H. J., Gao, Q., Tan, H. H., Jagadish, C., Paladugu, M., & Suvorova, A. A. Nano letters, 6(4), 599 (2006)

[**Kodambaka 2006**] Kodambaka, S., Tersoff, J., Reuter, M. C., & Ross, F. M. Physical review letters, 96(9), 096105 (2006)

[**Li 2008**] Li, Y., Della Valle, F., Simonnet, M., Yamada, I., & Delaunay, J. J. Nanotechnology, 20(4), 045501 (2008)

[**Li 2021**] D. Li, N. Akopian, arXiv:2107.05960 (2021)

[**Matteini 2015**] F. Matteini, G. Tütüncüoglu, H. Potts, F. Jabeen, A. Fontcuberta i Morral, Crystal Growth & Design 15, 3105 (2015)

[**Panciera 2020**] F. Panciera, Z. Baraissov, G. Patriarche, V. G. Dubrovskii, F. Glas, L. Travers, U. Mirsaidov, J.-C. Harmand, Nano Letters 20, 1669 (2020)

[**Priante 2013**] G. Priante, S. Ambrosini, V. G. Dubrovskii, A. Franciosi, S. Rubini, Crystal Growth & Design 13, 3976 (2013)

[**Ramdani 2010**] Ramdani, M. R., Gil, E., Leroux, C., André, Y., Trassoudaine, A., Castelluci, D., Kupka, R. Nano Letters 10, 1836 (2010)

[**Ramdani 2013**] M. R. Ramdani, J. C. Harmand, F. Glas, G. Patriarche, L. Travers, Crystal Growth & Design 13, 91 (2013)

[**Rudolph 2011**] D. Rudolph, S. Hertenberger, S. Bolte, W. Paosangthong, D. Spirkoska, M. Döblinger, M. Bichler, J. J. Finley, G. Abstreiter, G. Koblmüller, Nano Letters 11, 3848 (2011)

[**Spells 1936**] Spells, K. E. Proceedings of the Physical Society, 48(2), 299 (1936)

[**Thelander 2006**] C. Thelander, P. Agarwal, S. Brongersma, J. Eymery, L. F. Feiner, A. Forchel, M. Scheffler, W. Riess, B. J. Ohlsson, U. Gosele, L. Samuelson, Materials Today 9, 28 (2006)

[**Vainorius 2014**] N. Vainorius, D. Jacobsson, S. Lehmann, A. Gustafsson, K. A. Dick, L. Samuelson, M.-E. Pistol, Physical Review B 89, 165423 (2014).

[**Vainorius 2015**] N. Vainorius, S. Lehmann, D. Jacobsson, L. Samuelson, K. A. Dick, M.-E. Pistol, Nano Lett. 15, 2652−2656 (2015).

[**Vettori 2019**] M. Vettori, V. Piazza, A. Cattoni, A. Scaccabarozzi, G. Patriarche, P. Regreny, N. Chauvin, C. Botella, G. Grenet, J. Penuelas, A. Fave, M. Tchernycheva, M. Gendry, Nanotechnology 30, 084005(2019)

[**Vettori 2019b**] M. Vettori, A. Danescu, X. Guan, P. Regreny, J. Penuelas, M. Gendry, Nanoscale Advances 1, 4433 (2019)

[**Wang 2010**] Wang, Z. L Nano Today 5, 6 (2010)

[**Wu 2006**] H. Wu, W. Pan, Journal of the American Ceramic Society 89(2), 699 (2006)

[**Zhou 2010**] Z. Y. Zhou, C. X. Zheng, W. X. Tang, D. E. Jesson and J. Tersoff, Appl. Phys. Lett. 97, 121912 (2010)

[**Zhou 2017**] Chen Zhou, Kun Zheng, Zhi-Ming Liao, Ping-Ping Chen, Wei Lud and Jin Zou, J. Mater. Chem. C 5, 5257 (2017)

Figures

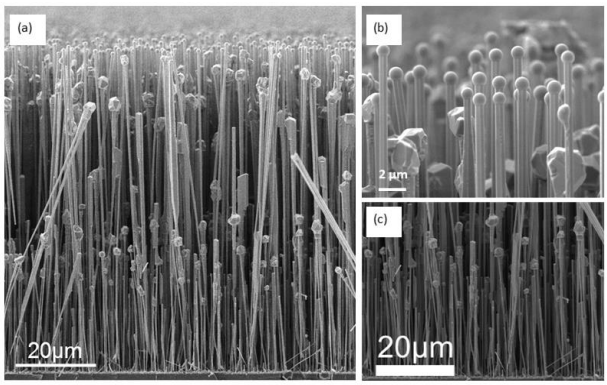

Fig 1: SEM side view of ultra-long GaAs NWs grown during 720 min (a). Two groups of NWs are clearly evidenced. In the first group the NWs exhibit a droplet on their top, which confirms the VLS growth mode (b) while in the second group the NWs are shorter and exhibit a GaAs crystallite on their top (c).

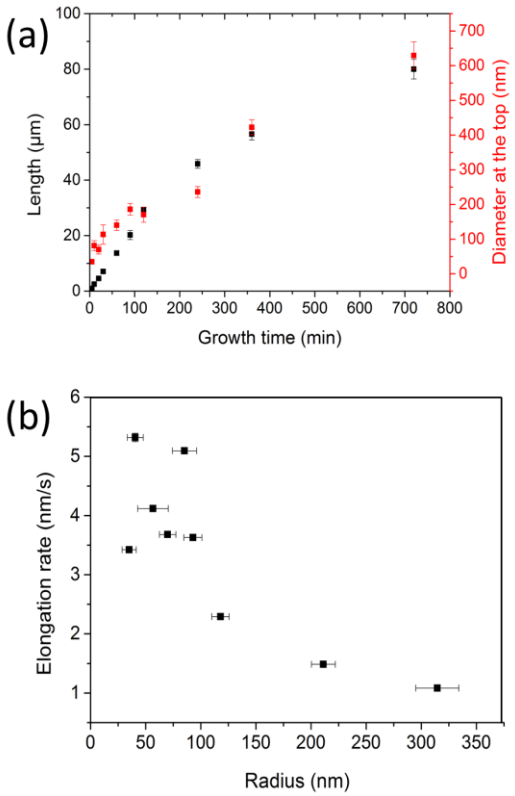

Fig 2: (a) Length and diameter of GaAs NWs as a function of the growth time. (b) Axial growth rate as function of the NW radius beneath the droplet.

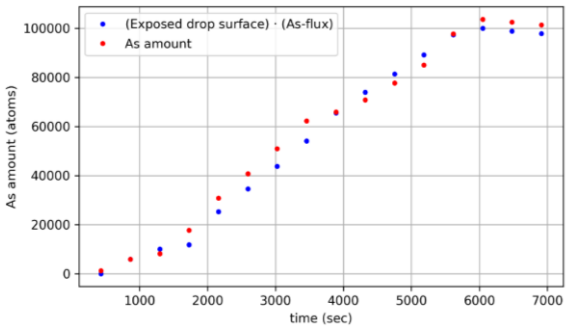

Fig 3: The evolution of the computed (equal) amount of As (or Ga) for each time interval $[k\Delta t, (k+1)\Delta t]$ for $k = 1 \ldots 16$ and $\Delta t = 432$ s (in red) and the amount of As entering the droplet by direct impingement (in blue) computed as the product between the fixed-value of As-flux equal to 1.7×10^7 atoms/(nm².s) and the time dependent surface of the droplet exposed to the As flux.

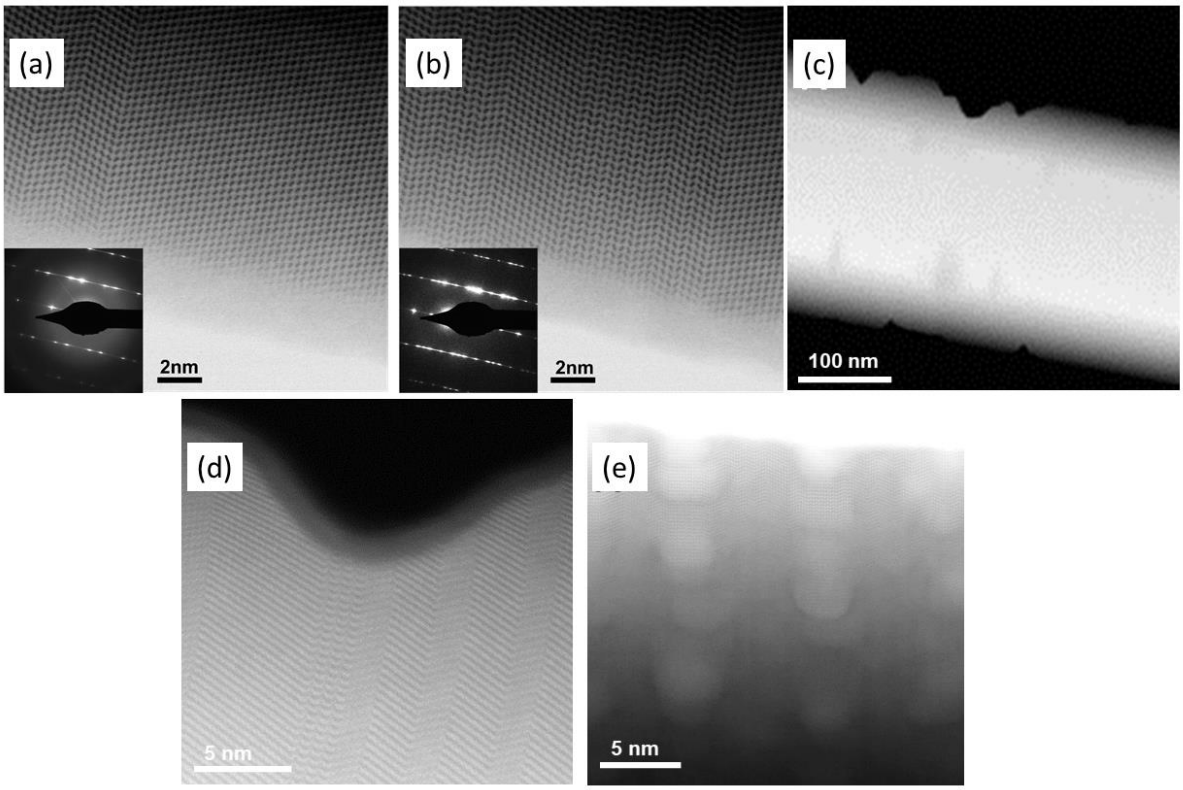

Fig 4: TEM images of: (a) twins in the ZB phase and (b) WZ inclusions. Insets: corresponding diffraction patterns. (c) TEM image of an ultra-long GaAs NW where notches can be observed and (d) the corresponding high resolution image where a WZ segment can be observed. (e) TEM image of the bottom an ultra-long GaAs NW where a high density of holes can be observed.

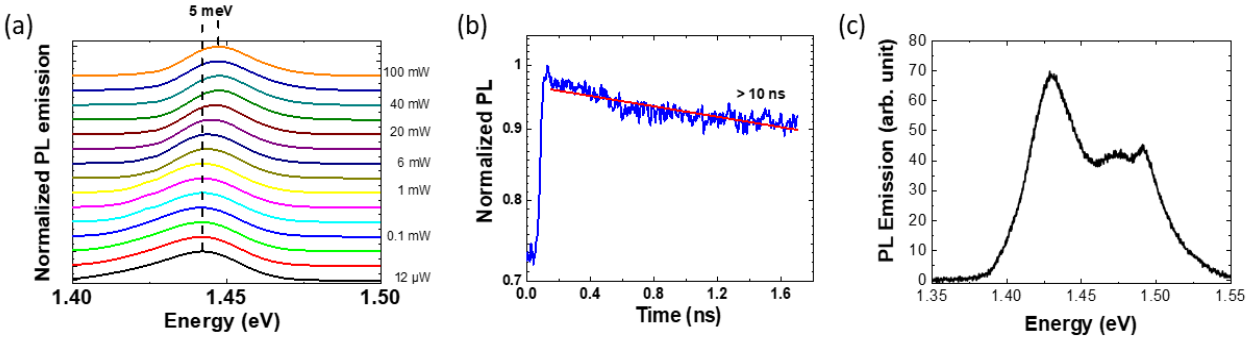

Fig 5: (a) PL spectra as a function of the excitation power at 14 K. (b) Decay time of the PL emission at 14 K. (c) µ-PL spectrum of a single NW at 10 K.

Supporting Information for:

Growing self-assisted GaAs nanowires up to 80 µm long by Molecular Beam Epitaxy

1. **Morphology of ultra-long NWs**
2. **Temperature profile of ultra-long NWs**
3. **TEM and SAED data of ultra-long NWs**
4. **PL as a function of the temperature**
5. **Growing ultralong nanowire under higher As flux**

1. Morphology of ultra-long NWs

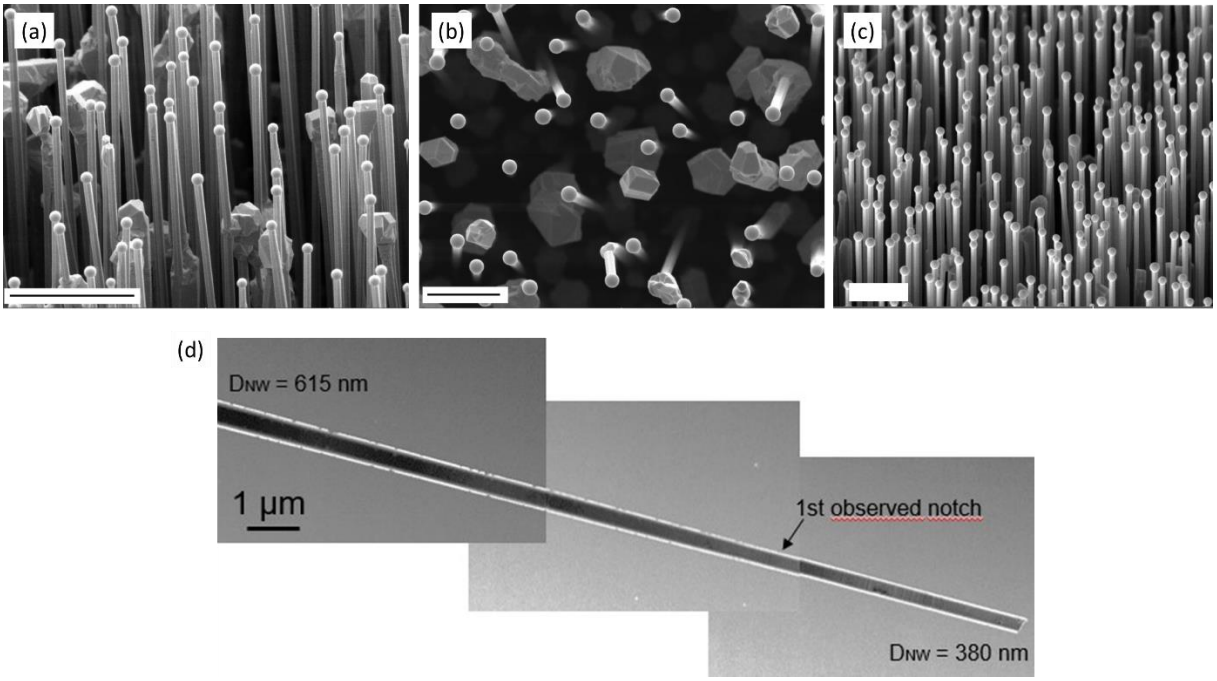

Fig S1: Scanning Electron Microscopy images of GaAs NWs. NWs were grown during 12 hours leading to a length up to 80 µm-long: (a) Bird eye view, the scale bar is 10 µm. (b) Top view, the scale bar is 5 µm. (c) Bird eye view of a sample grown during 2 hours. The scale bar is 5 µm (d) Transmission Electron Microscopy images showing the NW tapering (12 hours growth). The NW growth direction is [111].

2. Temperature profile in ultra-long NWs

To calculate the temperature at the tip of a cylindrical NW, we use the model developed by Frank Glas and Jean-Christophe Harmand in [**Glas 2006**]. This temperature is calculated numerically using the equation:

$$l = \Lambda \int_{\tau_l}^{1} \left[\frac{1}{10}(\tau^5 - {\tau_l}^5) - \frac{\alpha}{4}(\tau - \tau_l) + \left(\frac{r_0}{8\Lambda}\right)^2 {\tau_l}^8 \right]^{-1/2} d\tau$$

where $\tau_l = T_l/T_s$ with T_l the temperature at the tip of a NW of length l and $T_s = 883\ K$ the temperature of the substrate. The absorption α is assumed to be equal to the emissivity. At 610°C, we have $\epsilon \approx 0.3$ [**Timans 1992**]. The characteristic length Λ is equal to:

$$\Lambda = \sqrt{\frac{\kappa r_0}{8\epsilon\sigma T_s^3}}$$

where $r_0 = 100\ nm$ is the NW radius, σ the Stefan-Boltzmann's constant and κ the thermal conductivity. This thermal conductivity is equal to 19 $Wm^{-1}K^{-1}$ at 883 K for bulk GaAs [**Maycock 1967**]. However, it is known that κ can have a smaller value in semiconducting NWs. In Ref [**Martin 2010**], it is theoretically predicted that, for a 100 nm radius GaAs NW, κ is decreased by a factor of two in the case of a NW with ideally smooth surfaces and could be reduced by a factor of 10 in the case of a NW with rough surfaces. Fig S2 shows the temperature at the tip of a 100 nm radius GaAs NW as a function of the NW length for three different thermal conductivities: 19 $Wm^{-1}K^{-1}$ (bulk GaAs), 10 $Wm^{-1}K^{-1}$ (NW with smooth surfaces), 2 $Wm^{-1}K^{-1}$ (NW with rough surfaces). We can see on this graph that the temperature drop is at least of 45 K for an 80 µm long NW.

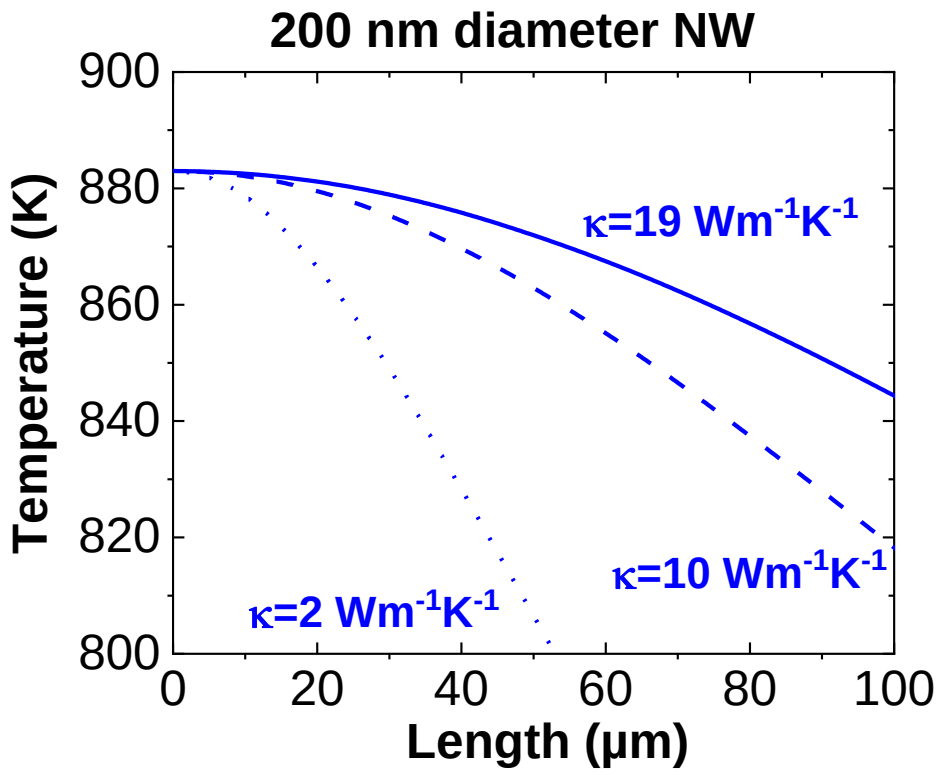

Fig S2: Temperature at the tip of the NW as a function of its length, for different thermal conductivities.

3. TEM and SAED data of ultra-long NWs

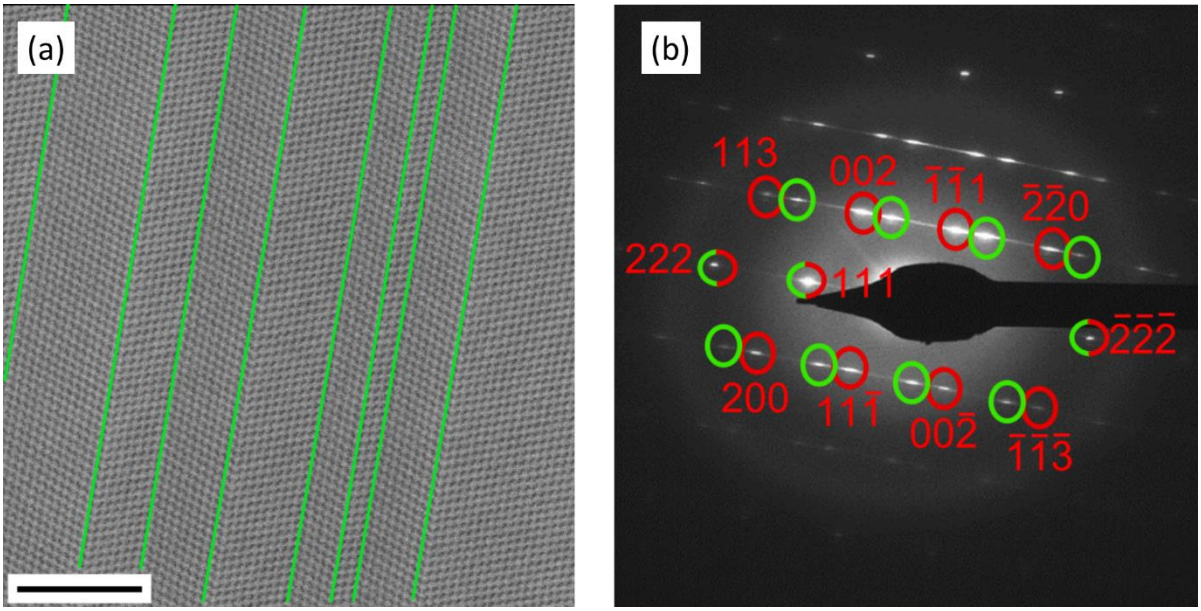

Fig S3: (a) High resolution TEM image of a pure ZB section of an ultra-long NW. The green lines highlight the twin planes. The scale bar is 5 nm. (b) Diffraction pattern showing the two ZB variants (in red and green).

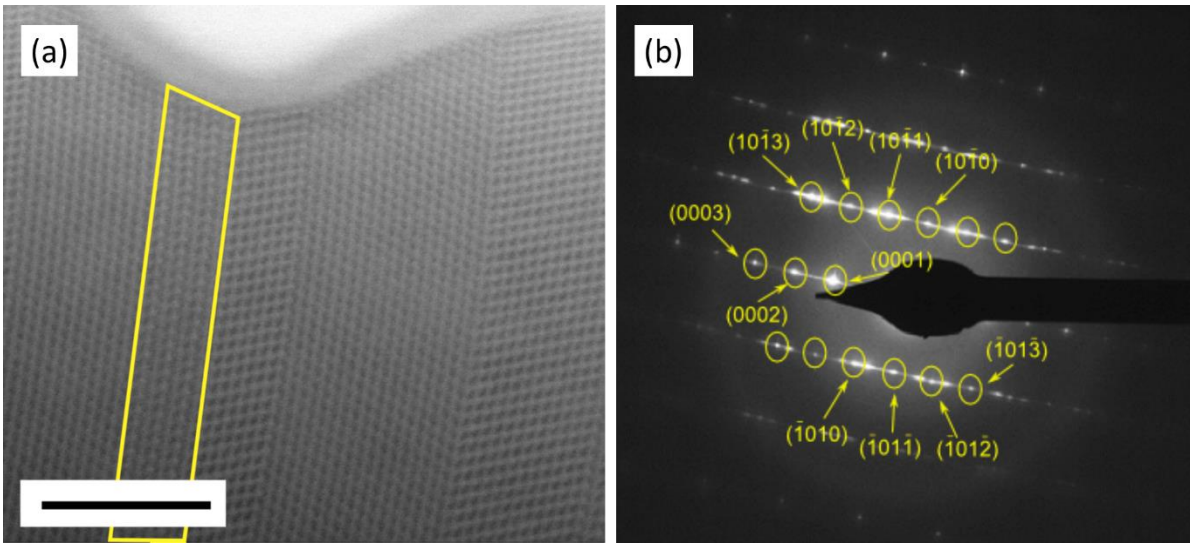

Fig S4: (a) High resolution TEM image of a WZ segment (highlighted in yellow) surounded by ZB sections in an ultra-long NW. The scale bar is 5 nm. (b) Diffraction pattern highlighting the presence of the WZ phase.

4. Photoluminescence as a function of the temperature

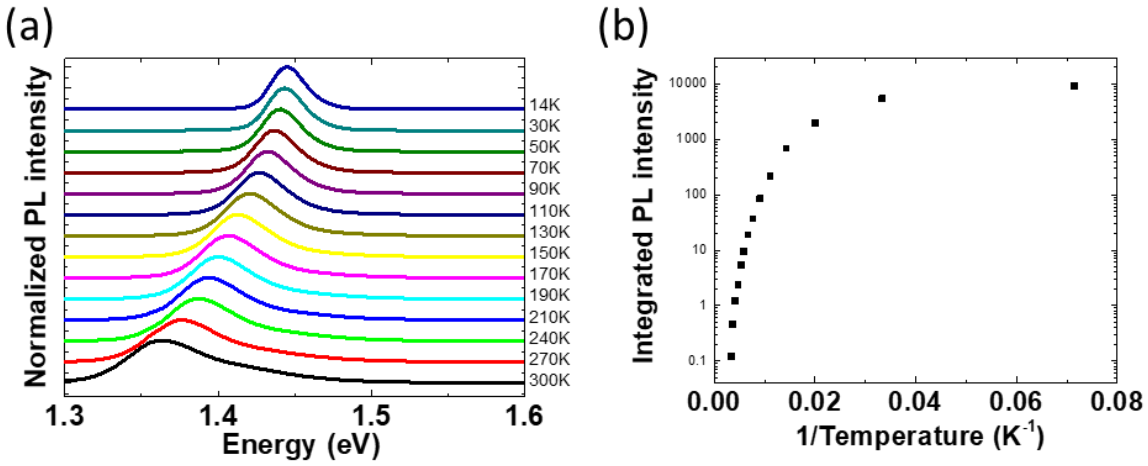

Fig S5: (a) Normalized PL spectra as a function of the temperature. (b) Integrated PL intensity as a function of the temperature

A PL redshift of 80 meV is observed from 14 K to 300 K, smaller than the 96 meV expected PL shift of the ZB GaAs bulk material [**Vurgaftman 2001**]. At room temperature, a shoulder located at 1.42 eV, associated to the ZB GaAs emission, is observed, as a consequence of the thermal activation of the electrons from the WZ segment towards the ZB sections. As far as the PL integrated intensity is concerned, a decrease by more than 4 orders of magnitude is reported when the temperature is increased from 12 K to 300 K. The fact that the NWs are unpassivated could explain this result. A 5 orders of magnitude PL decrease has already been reported for unpassivated gold catalyzed ZB GaAs NWs [**Breuer 2011**]. This strong decrease is also probably related to the carrier separation. The thermal activation of non-radiative decay channels induces a competition with the radiative recombinations. Due to the weak radiative decay rate, the non-radiative processes can easily take over the radiative ones.

5. Growing ultralong nanowire under higher As flux

Tuning the As flux during the growth of self-assisted GaAs NWs is known to produce a modification of their morphology and crystal phase. By increasing the As molecular beam flux we obtained NWs without inverse tapering. It is expected the crystalline structure can be modified by careful adjustment of the V/III ratio.

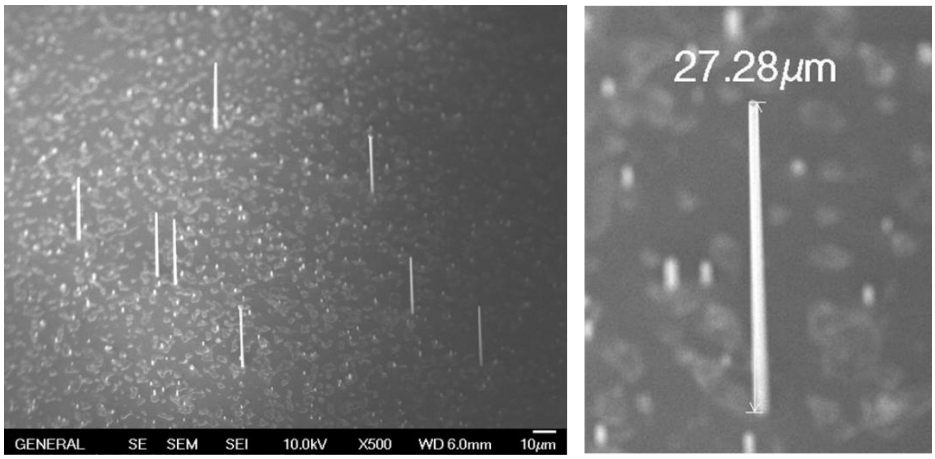

Figure S6: SEM image of ultralong NWs grown during 6 hours with higher As flux.

Bibliography

[**Breuer 2011**] S. Breuer, C. Pfüller, T. Flissikowski, O. Brandt, H. T. Grahn, L. Geelhaar, H. Riechert, Nano letters, 11, 1276-1279 (2011)

[**Glas 2006**] Glas, F., & Harmand, J. C. Physical Review B, 73(15), 155320 (2006)

[**Martin 2010**] P. N. Martin, Z. Aksamija, E. Pop and U. Ravaioli, Nano Lett. 10, 1120–1124 (2010)

[**Maycock 1967**] P. D. Maycock, Solid-State Electronics 10, 161-168 (1967)

[**Timans 1992**] P. J. Timans, J. Appl. Phys. 72, 660 (1992)

[**Vurgaftman 2001**] I. Vurgaftman, J. R. Meyer, L. R. Ram-Mohan, Journal of Applied Physics 89, 5815 (2001)